International Journal of Minerals, Metallurgy and Materials
Volume 24, Number 8, August 2017, Page 918
DOI: 10.1007/s12613-017-1478-2

Studies on induction hardening of powder-metallurgy-processed Fe–Cr/Mo alloys

Sandeep Chauhan[1)], *Vikas Verma*[2)], *Ujjwal Prakash*[2)], *P.C. Tewari*[1)], *and Dinesh Khanduja*[1)]

1) Department of Mechanical Engineering, National Institute of Technology, Kurukshetra 136119, India
2) Department of Metallurgical & Materials Engineering, Indian Institute of Technology, Roorkee 247667, India
(Received: 28 November 2016; revised: 1 April 2017; accepted: 5 April 2017)

Abstract: Induction hardening of dense Fe–Cr/Mo alloys processed via the powder-metallurgy route was studied. The Fe–3Cr–0.5Mo, Fe–1.5Cr–0.2Mo, and Fe–0.85Mo pre-alloyed powders were mixed with 0.4wt%, 0.6wt%, and 0.8wt% C and compacted at 500, 600, and 700 MPa, respectively. The compacts were sintered at 1473 K for 1 h and then cooled at 6 K/min. Ferrite with pearlite was mostly observed in the sintered alloys with 0.4wt% C, whereas a carbide network was also present in the alloys with 0.8wt% C. Graphite at prior particle boundaries led to deterioration of the mechanical properties of alloys with 0.8wt% C, whereas no significant induction hardening was achieved in alloys with 0.4wt% C. Among the investigated samples, alloys with 0.6wt% C exhibited the highest strength and ductility and were found to be suitable for induction hardening. The hardening was carried out at a frequency of 2.0 kHz for 2–3 s. A case depth of 2.5 mm was achieved while maintaining the bulk (interior) hardness of approximately HV 230. A martensitic structure was observed on the outer periphery of the samples. The hardness varied from HV 600 to HV 375 from the sample surface to the interior of the case hardened region. The best combination of properties and hardening depth was achieved in case of the Fe–1.5Cr–0.2Mo alloy with 0.6wt% C.

Keywords: Fe–Cr/Mo alloys; powder metallurgy; sintered density; tensile strength; induction hardening; case depth

1. Introduction

Powder metallurgy (P/M) is an efficient processing technique because of its unique advantage of producing densified alloy steels with improved mechanical properties. It produces near-net-shape components and is used for making high-performance components in automotive industry [1–2]. Even brittle Ni_3Al intermetallic compounds can be fabricated by the P/M technology [3]. Alloying elements and P/M process parameters affect the structure and properties of P/M steels. Cr–Mo alloy steels are used in high-temperature applications because of their excellent creep resistance at high temperatures. High-temperature sintering of Cr–Mo steels results in better mechanical properties.

Yu explained the diffusion behavior of Cr and Mo during sintering of Fe–3Cr–0.5Mo alloy on the basis of continuous cooling transformation diagrams. The Fe–Cr–Mo alloys containing 0.3wt%–0.5wt% C were sintered at 1393 K with heating and cooling rates ranging from 0.8 to 2 K/s; he observed a bainitic and martensitic microstructure [4]. Kandavel *et al.* processed an Fe–0.5C alloy at various loads and at a sintering temperature of (1273 ± 10) K, which was maintained for 2 h in a nitrogen-purged 3.5-kW muffle furnace. The maximum density of 97% was obtained in the sintered samples prepared at a cold upset of 550 kN at a high aspect ratio of 1.3 [5]. Sandeep *et al.* processed Fe–C alloy steel under optimum conditions of a compaction load of 700 MPa and a sintering temperature of 1373 K for 1 h. The low density of the processed alloy was attributed to the low compressibility of powder constituents [6].

Different alloying constituents have been used in alloy steels to improve their physical and mechanical properties. The addition of 0.5wt% Cr to the Fe–4Ni–1.5Cu–0.5Mo–0.5C sintered steel results in improved mechanical properties, as reported by Wu *et al.* [7]. The steel was compacted using a 500-MPa load and was sintered at 1523 K. An increase of 38% in ultimate tensile strength and a decrease of 15% in impact energy were observed. Amador *et al.* [8] added Mo,

Corresponding author: Sandeep Chauhan E-mail: sandeep2140@gmail.com

a ferrite stabilizer, to alloy steel and found that it induces solid–solution strengthening and enhances the hardenability of steel. These effects were confirmed by Engstrom *et al.* and by Shigeru *et al.* [9–10]. Kremel *et al.* [11] processed the sintered Cr–Mo alloy containing 0.2wt%–0.5wt% C at 1393 and 1473 K and found strong interparticle bonding at 1473 K that resulted in high hardness. Marcu *et al.* [12] processed the Fe–3Cr–0.5Mo alloy with 0.6wt% C compacted at 700 MPa and sintered at 1393 and 1523 K with a cooling rate of 40 K/min and achieved an improvement of 37% in tensile strength upon increasing the sintering temperature from 1393 to 1523 K. Hrubovcakova *et al.* [13] studied sintering of the Fe–Cr–Mo pre-alloyed powder with additions of 0.5wt%, 0.6wt% and 0.8wt% C in 90%N_2–10%H_2 sintering atmosphere using continuous monitoring of the exhaust gas composition (CO, CO_2, and H_2O) and elucidated the relationships between the density (6.5–7.4 g/cm^3), sintering temperature (1393 and 1473 K), and the heating and cooling rates (10 and 50 K/min). Specifically, the higher sintering temperature (1473 K) and a density of 7.0 g/cm^3 resulted in a greater than 80% decrease in the relative oxygen content. Complete reduction of chromium oxides was not observed for the Fe–Cr–Mo alloy with 0.4wt% C sintered at 1393 K for 1 h [14].

The aforementioned literatures show that various researchers have attempted to improve the properties of alloy steel by adding different alloying elements and varying the P/M process parameters. We noted that faster cooling rates were used during sintering of Fe–Cr/Mo alloys. In the present work, we processed Fe–Cr/Mo alloys using slower cooling rates and investigated the properties of the obtained samples.

Induction hardening is one of the best methods to further enhance the surface hardness of Fe–Cr/Mo alloys, thereby improving their performance. In induction hardening, the surface is hardened to a required depth within a short time using high-temperature heating and water quenching, thus avoiding scaling [15]. Also, the inner core of the P/M product remains unaffected, allowing the samples to retain their toughness, thereby restricting crack propagation. Induction hardening utilizes the principle of electromagnetic induction to heat the surface layer of a workpiece. More than 70% of the current generated by the electromagnetic induction flows in a thin surface layer. Induction hardening enables control of the mechanical properties of metal parts by imparting surface hardness while the core retains the original structure, resulting in high hardness [15]. Palaniradja *et al.* [16] carried out induction hardening on specimens of wrought steel materials—grades AISI 1040, AISI 4140, AISI 4340, AISI 1055, AISI 6150, and AISI 9255, with carbon contents from 0.35wt% to 6.0wt%, and studied the microstructures of the products. Their results showed that the microstructure transformed from austenite to martensite and that the specimens achieved hardness in the range of HRC 55–HRC 65 when the power potential was 0.85 kW/cm^2, the scan speed was 1.34 m/min, and the quenching flow rate was 15 L/min. Kusmoko *et al.* [17] achieved a high surface hardness value of HV 685 for AISI 1045 wrought steel whose surface was heated at 1473 K for 2 s before the specimen was quenched in water.

A survey of literatures indicates that induction hardening studies have been carried out mostly on wrought steel, whereas literatures regarding induction hardening of the P/M processed alloy steel are limited. The prevailing porosity in the P/M-processed samples may restrict effective hardening because proper heating and cooling parameters must be used to achieve the desired hardness and effective case depth during the induction hardening process of alloy steel [18]. In the case of porous samples, a higher power setting is normally required to achieve a given depth of hardening compared to that used for a wrought material with similar composition. Furthermore, because heat dissipates rapidly and more carbon diffusion occurs, rapid water quenching is necessary to achieve the required case depth and hardness [19]. In the present work, we attempted to induce induction hardening in the P/M-processed Fe–Cr/Mo alloy steel.

2. Experimental

Water-atomized powders of Fe–Cr/Mo alloys were supplied by Hoganas India. Three alloy compositions, Fe–3Cr–0.5Mo, Fe–1.5Cr–0.2Mo, and Fe–0.85Mo, were used in this study. The pre-alloyed powders exhibited an average particle size between 110 and 130 μm. Ultra-fine graphite powder with a particle size ranging from 2 to 3 μm was added to the selected compositions. The alloy powders were mixed with 0.4wt%, 0.6wt%, and 0.8wt% C for 1 h in a ball mill (10:1 ratio of ball to metal). The mixed powders were compacted at 500, 600, and 700 MPa using the die shown in Fig. 1. A mixture of acetone and stearic acid was used for die wall lubrication. The green compacts of dog-bone shape were sintered at 1473 K for 1 h in a tubular furnace under a gas mixture of (90vol%N_2 + 10vol%H_2). The diameter of the tube where the samples were placed for sintering in the tube furnace was 50 mm, and the effective heating length was approximately 200 mm. The sintered compacts were cooled to room temperature at a cooling rate of 6 K/min. These compacts conform to ASTM E8-04 for P/M tensile samples.

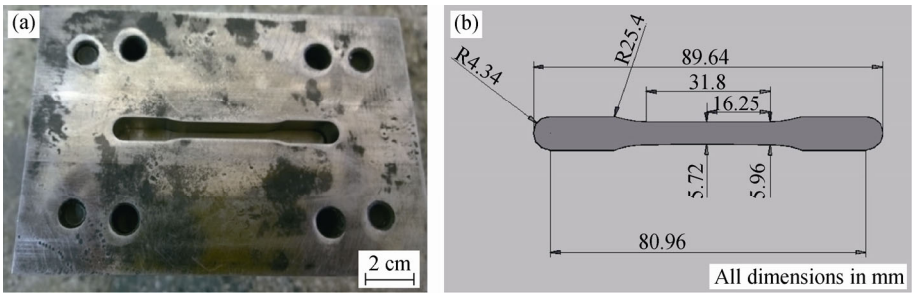

Fig. 1. Dog-bone shape: (a) die; (b) dimensional details.

The density of the green and sintered samples was measured by weight and volume measurements. The carbon content of the sintered compacts was determined using a Leco carbon and sulfur analyzer. Transverse sections were cut from the sintered samples, mechanically polished to a 1-μm-grade alumina powder finish, and etched with 2vol% nital solution for observation by optical microscopy using a Leica 5000M microscope. Their surfaces were further examined using a Quanta 200 FEI scanning electron microscope. Hardness measurements were carried out on polished sample sections using a 49-N load in a FIE VM50 Vickers hardness testing machine. Tensile tests were performed on the sintered dog-bone-shaped samples at a strain rate 0.5 mm/min using a computer-controlled Hounsfield test instrument (H25KS) with a 25-kN capacity.

The alloys with 0.4wt% and 0.6wt% C were selected for induction hardening studies. The cylindrical samples of 32 mm in diameter and 50 mm in height were also prepared in a circular die using the alloy with 0.6wt% C and a 700-MPa load. These samples were similarly sintered and then subjected to induction hardening in a 75-kW A.B. Electricals induction hardening unit. The induction hardening was carried out using a 2.0 kHz frequency for 2–3 s on alloy steel specimens, which raised its outer periphery surface temperature to approximately 1223 K; further quenching was carried out using water spray to increase the case depth and hardness. Transverse sections were cut from the center of the hardened samples. The sectioned samples were polished, and the case depth was examined using an Omnitech (MVH-II) microhardness tester. The polished sections were subsequently etched for optical microscopy and scanning electron microscopy (SEM) studies. A Rigaku Smartlab X-Ray diffractometer (G8, Bruker, Germany) was used for phase identification.

3. Results and discussion

3.1. X-ray diffraction and density measurements

The Fe–Cr/Mo alloy steel specimens with specific compositions Fe–3Cr–0.5Mo, Fe–1.5Cr–0.2Mo, and Fe–0.85Mo were processed via the P/M route. The density of the dog-bone-shaped sintered compacts ranged from 6.8 to 7.25 g/cm^3. The carbon content of the sintered compacts was found to range from 0.30wt% to 0.68wt%. These results are summarized in Table 1. An N_2–H_2 atmosphere enables the successful sintering of Cr-alloyed P/M steels [20]. The highest density was observed in samples prepared using the compaction pressure of 700 MPa. Ferrite (λ) and cementite (μ) peaks are observed in the XRD patterns of the sintered samples (Fig. 2(a)). The patterns of the induction-hardened samples reveal the martensite (α) peaks (Fig. 2(b)).

Table 1. Density of green and sintered Fe–3Cr–0.5Mo, Fe–1.5Cr–0.2Mo, and Fe–0.85Mo dog-bone-shaped compacts

Graphite content / wt%	Compaction load / MPa	Green density / (g·cm^{-3})			Sintered density / (g·cm^{-3})		
		Fe–3Cr–0.5Mo	Fe–1.5Cr–0.2Mo	Fe–0.85Mo	Fe–3Cr–0.5Mo	Fe–1.5Cr–0.2Mo	Fe–0.85Mo
0.4	500	6.81	6.83	6.80	6.84	6.87	6.82
	600	7.12	7.13	6.98	7.14	7.14	7.02
	700	7.18	7.20	7.08	7.18	7.22	7.10
0.6	500	6.82	6.84	6.80	6.83	6.88	6.81
	600	7.14	7.14	7.01	7.15	7.17	7.04
	700	7.20	7.22	7.10	7.21	7.25	7.12
0.8	500	6.81	6.86	6.80	6.82	6.87	6.81
	600	7.15	7.16	7.04	7.17	7.18	7.06
	700	7.18	7.20	7.11	7.20	7.22	7.14

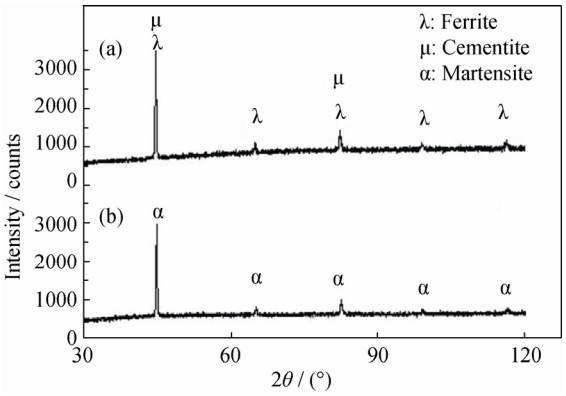

Fig. 2. XRD patterns of the Fe–1.5Cr–0.2Mo alloys with 0.6wt% C: (a) after sintering; (b) after induction hardening.

3.2. Microstructure and mechanical behavior of sintered alloys

Observations of the microstructure of the samples with 0.8wt% C reveal the presence of graphite at prior particle boundaries (Fig. 3). Ferrite and pearlite are observed in the microstructure of sintered alloys, whereas Cr/Mo carbides are observed at ferrite boundaries (Fig. 4). The microstructure of Fe–Cr/Mo–0.6C consists of the mixture of ferrite and pearlite with some carbides at the boundaries, whereas relatively more pearlite and carbide are observed in the Fe–Cr/Mo alloy with 0.8wt% C because of the higher carbon content of the alloy. Also, some graphite is observed at the boundary, which weakens the bonds among grains and lowers the strength in the case of 0.8wt% C.

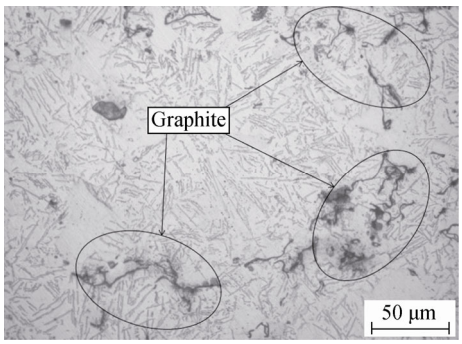

Fig. 3. Microstructure of the sintered Fe–0.85Mo alloy with 0.8wt% C.

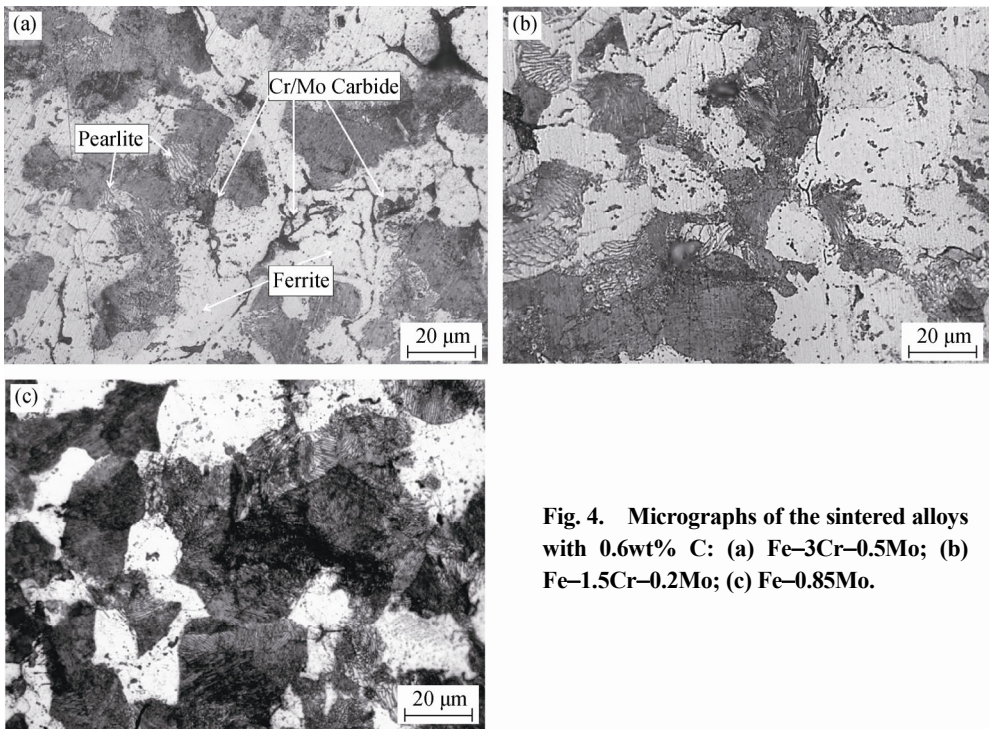

Fig. 4. Micrographs of the sintered alloys with 0.6wt% C: (a) Fe–3Cr–0.5Mo; (b) Fe–1.5Cr–0.2Mo; (c) Fe–0.85Mo.

The regions near ferrite boundaries observed in SEM micrographs of the sintered Fe–3Cr–0.5Mo alloy specimens were examined in conjunction with energy-dispersive X-ray spectroscopy (EDS) analysis. The EDS results indicate the presence of alloyed carbides at these boundaries (Fig. 5).

The mechanical properties of the Fe–Cr/Mo alloy are strongly influenced by the carbon addition, compaction load, and sintering temperature. The results of hardness and tensile tests of the processed Fe–3Cr–0.5Mo, Fe–1.5Cr–0.2Mo, and Fe–0.85Mo alloy steel specimens with different carbon contents are summarized in Table 2. The carbon content also affects the hardness and tensile strength. The hardness and tensile strength were lower in the alloys with 0.8wt% C as a consequence of graphite particles at prior particle bounda-

ries. Thus, the samples with 0.4wt% and 0.6wt% C were selected for subsequent induction hardening studies. A higher volume fraction of pearlite and the absence of graphite or presence of very little graphite at prior particle boundaries in Fe–1.5Cr–0.2Mo alloys resulted in a higher hardness and a higher ultimate tensile strength (Table 2). In the case of alloys with 0.8wt% C, graphite is present at prior particle boundaries, which decreases the mechanical properties of the sintered alloy. Chauhan *et al.* [21] analyzed the Fe–3Cr–0.5Mo alloys with 0.4wt% and 0.8wt% C after compaction under a 650-MPa load and sintering at 1393 or 1473 K for 1 h with a cooling rate of 3.5 or 6 K/min; they found that the increase in carbon content adversely affected the mechanical properties. In the present work, the hardness (HV 233), ultimate tensile strength (457.7 MPa), and percentage elongation (6.4%) are maximum for the Fe–1.5Cr–0.2Mo–0.6C alloy compacted at 700 MPa and sintered at 1473 K. Such a high sintering temperature may also facilitate carbide dissolution and is responsible for the higher pearlite/carbide contents in alloys sintered at 1473 K [14]. The higher pearlite/carbide contents, in turn, also improve the mechanical properties. At higher Cr/Mo contents, more alloy carbide formation is observed at ferrite boundaries. Thus, both Fe–3Cr–0.5Mo and Fe–0.85Mo alloys exhibit lower strength and ductility compared to the Fe–1.5Cr–Mo alloy with 0.6wt% C.

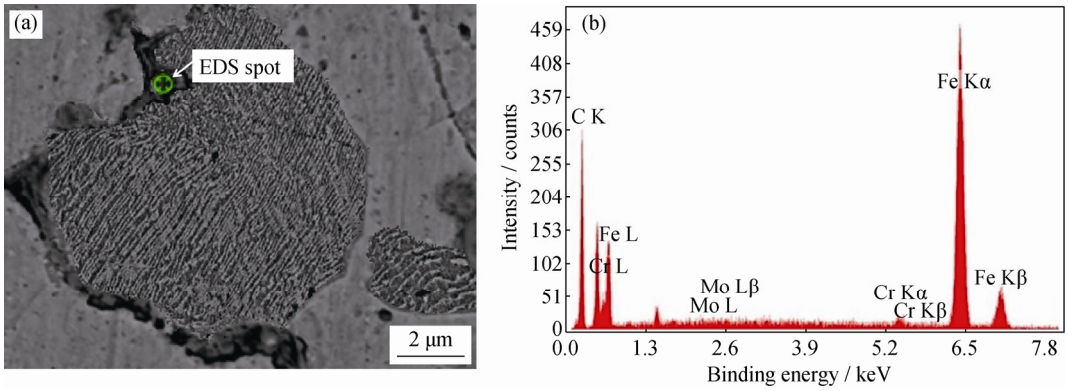

Fig. 5. SEM image showing the spot analyzed by EDS (a) and a typical EDS spectrum of alloy carbides at the ferrite boundary in Fe–3Cr–0.5Mo alloy (b).

Table 2. Mechanical properties of sintered alloys

Graphite content / wt%	Compaction load / MPa	Hardness, HV			Tensile strength / MPa			Elongation / %		
		Fe–3Cr–0.5Mo	Fe–1.5Cr–0.2Mo	Fe–0.85Mo	Fe–3Cr–0.5Mo	Fe–1.5Cr–0.2Mo	Fe–0.85Mo	Fe–3Cr–0.5Mo	Fe–1.5Cr–0.2Mo	Fe–0.85Mo
0.4	500	189	145	152	280.2	289.3	277.2	1.4	1.8	1.6
	600	215	190	185	310.1	360.7	305.1	2.4	3.1	2.8
	700	230	195	194	340.5	392.1	324.1	3.0	3.5	3.1
0.6	500	202	191	188	339.5	343.4	231.6	1.3	2.3	1.9
	600	223	225	210	382.1	432.9	388.2	1.9	4.1	2.9
	700	231	233	220	418.2	457.7	401.0	2.2	6.4	3.5
0.8	500	182	186	190	252.6	270.3	239.7	1.2	1.8	1.6
	600	195	209	212	288.6	325.8	299.7	1.5	2.1	1.9
	700	201	218	217	298.9	352.3	312.2	1.8	2.8	2.3

3.3. Induction-hardened sintered Fe–Cr/Mo alloys

Decarburization occurs during sintering, which leads to a lower carbon content of sintered samples, as confirmed by the Leco carbon and sulfur analyzer. The 0.6wt% C compacts contain approximately 0.5wt% C after sintering, whereas the 0.4wt% C compacts contain approximately 0.3wt% carbon after sintering. The decarburization tendency of sintered samples is due to exposure to elevated temperatures during sintering for relatively longer times. Induction hardening at 2.0 kHz for 2–3 s on alloy steel specimens in-

creased their outer periphery surface temperature to approximately 1223 K; further quenching using water spray resulted in high case-depth and hardness. A martensitic structure could not be obtained after induction hardening in alloys with 0.4wt% C because of the low carbon content (Fig. 6). After sintering, the sample contained only 0.3wt% C. A martensitic structure was observed on the outer periphery of the samples containing 0.6wt% C (Fig. 7). The effective case depth (ECD) for Fe–1.5Cr–0.2Mo alloy steel was 2 mm, whereas the ECD for Fe–3.0Cr–0.5Mo and Fe–0.85Mo alloys was 1.5 and 1.75 mm, respectively. This difference may be due to larger amounts of Cr/Mo in these alloys.

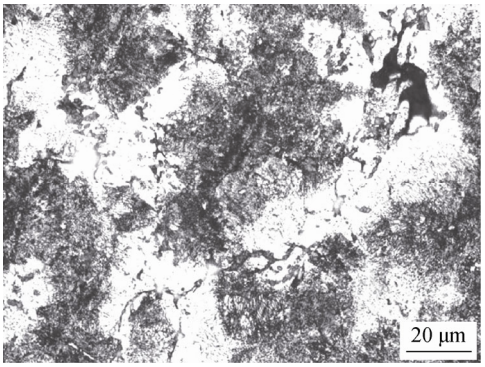

Fig. 6. Micrograph of the induction-hardened Fe–1.5Cr–0.2Mo alloy with 0.4wt% C, comprising ferrite and pearlite, but no martensite, indicating insufficient hardenability.

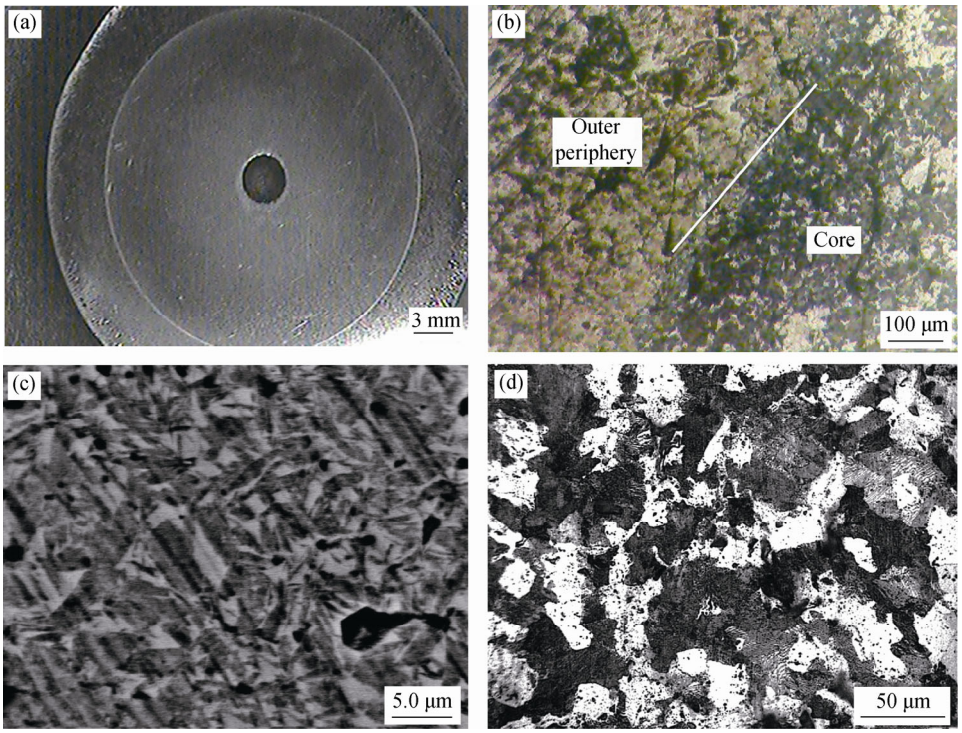

Fig. 7. Micrographs of the induction-hardened Fe–1.5Cr–0.2Mo alloy with 0.6wt% C: (a) low-magnification image of the polished sample (sample diameter = 32 mm); (b) transition zone showing the core and the outer periphery; (c) SEM micrograph of the periphery, showing the martensitic structure; (d) optical micrograph of the core of the sample, showing ferrite and pearlite.

In all of the samples, a transition from martensitic (effective case depth) to ferritic + martensitic structure (total case depth) from the surface to the core of the samples was observed (Fig. 8). This transition leads to a decrease of hardness, as shown in Fig. 9. The constant induction parameters used resulted in a difference in ECD, as observed for the specimens of different compositions. The ECD is the lowest when both Cr and Mo are high (i.e., in the case of Fe–3Cr–0.5Mo). The ECD is the highest when the Mo and Cr contents are low (i.e., in the case of Fe–1.5Cr–0.2Mo). Mo and Cr both are ferrite stabilizers; however, Mo is more effective in raising the eutectoid temperature [22]. The ECD is lower in the Fe–0.85Mo alloy than in the Fe–1.5Cr–0.2Mo alloy. Increasing the Mo content from 0.2wt% to 0.85wt% may overcome the effect of eliminating Cr. A variation in hardness (HV 600 to HV 375) was observed from the sample surface to the interior of the case-hardened region (Fig. 9), whereas the bulk (interior) hardness remained approximately HV 230. This difference in behavior may be due to variation of the cooling rate from the periphery to the interior of the samples during hardening. The sintered Fe–1.5Cr–0.2Mo alloy with 0.6wt% C exhibits a high ten-

sile strength of 457.7 MPa, an elongation of 6.4%, and a hardness of HV 233. After induction hardening, the alloy exhibits a maximum hardness of HV 600 and a case depth of 2.5 mm. Thus, among the studied alloys, the Fe–1.5Cr–0.2Mo alloy with 0.6wt% C is the best suitable for automobile gears and engine parts.

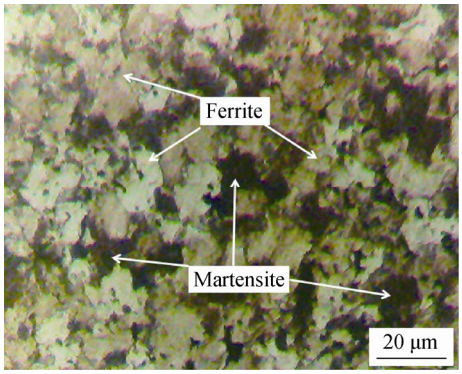

Fig. 8. Micrograph of the region near the transition zone, showing the ferritic and martensitic structure.

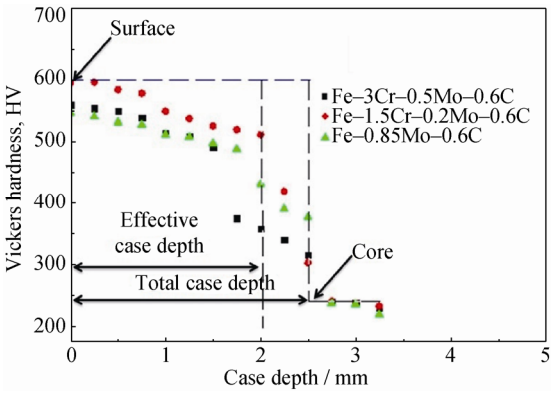

Fig. 9. Surface hardness variations from the surface to the core of Fe–3Cr–0.5Mo, Fe–1.5Cr–0.2Mo, and Fe–0.85Mo alloys, showing the sharp decrease in hardness after 2-mm case depth.

4. Conclusions

(1) A high density was observed in the samples prepared using a compaction pressure of 700 MPa.

(2) Ferrite and pearlite were observed in the microstructure and Cr/Mo carbides were observed at ferrite boundaries of the sintered alloys. In addition, the presence of graphite at prior particle boundaries was also observed in the sintered alloys with 0.8wt% C.

(3) At higher Cr/Mo contents, increased alloy carbide formation was observed at ferrite boundaries. Thus, both the Fe–3Cr–0.5Mo and Fe–0.85Mo alloys exhibit lower strength and lower ductility compared to the Fe–1.5Cr–Mo alloy with 0.6wt% C.

(4) Martensitic structure was not observed after induction hardening in alloys with 0.4wt% C. This lack of hardening is attributed to the low hardenability and the decrease in carbon content (>0.4wt% C) after sintering.

(5) Induction hardening of the Fe–1.5Cr–0.2Mo alloy with 0.6wt% C results in a maximum hardness of HV 600 and a maximum case depth of 2.5 mm.

(6) The ECD of the Fe–1.5Cr–0.2Mo alloy steel is 2 mm, whereas the ECD of the Fe–3.0Cr–0.5Mo and Fe–0.85Mo alloys is 1.5 and 1.75 mm, respectively. This difference may be due to the greater amounts of Cr/Mo in these alloys.

Acknowledgements

The authors would like to acknowledge Uniparts India Limited Noida, India for induction hardening. Hoganas Pune, India provided pre-alloyed Fe–Cr/Mo powders and Oxeeco, Hyderabad, India provided graphite powder free of cost for this work. One of the authors (SC) acknowledges the support of the MHRD fellowship from Government of India.

References

[1] R.M. German, *Powder Metallurgy and Particulate Materials Processing*, Metal Powder Industries Federation, Princeton, New Jersey, USA, 2005, p. 2.

[2] A. Salak, *Ferrous Powder Metallurgy*, Cambridge International Science Publishing, Cambridge, United Kingdom, 1997, p. 1.

[3] L.Y. Sheng, F. Yang, T.F. Xi, J.T. Guo, and H.Q. Ye, Microstructure evolution and mechanical properties of Ni_3Al/Al_2O_3 composite during self-propagation high-temperature synthesis and hot extrusion, *Mater. Sci. Eng., A*, 555(2012), p. 131.

[4] Y. Yu, Thermodynamic and kinetic behaviours of Astaloy CrM, [in] *PM World Congress & Exhibition*, Kyoto, Japan, 2000.

[5] T.K. Kandavel, T. Panneerselvam, and P. Karthikeyan, Optimization of deformation and densification properties of the sintered plain carbon steel, *Mater. Manuf. Processes*, 30(2015), No. 10, p. 1240.

[6] Sandeep, U. Prakash, P.C. Tewari, and D. Khanduja, Analysis of powder metallurgy process parameters for relative density of low carbon alloy steel using design of experiments tool, *Appl. Mech. Mater.*, 592-594(2014), p. 72.

[7] M.W. Wu, L.C. Tsao, and S.Y. Chang, The influences of chromium addition and quenching treatment on the mechanical properties and fracture behaviors of diffusion-alloyed powder metal steels, *Mater. Sci. Eng. A*, 565(2013), p. 196.

[8] D.R. Amador and J.M. Torralba, Study of PM alloyed steels with Ni–Cu prealloyed powders, *J. Mater. Process. Technol.*, 143-144(2003), p. 781.

[9] U. Engstrom, C. Lindberg, and J. Tengzelius, Powders and processes for high performance PM steels, *Powder Metall.*, 35(1992), No. 1, p. 67.

[10] S. Unami and Y. Ozaki, Molybdenum hybrid-alloyed steel powder for high fatigue strength sintered parts using mesh-belt sintering furnace, *JFE Tech. Rep.*, 2011, No. 16, p. 65.

[11] S. Kremel, H. Danninger, and Y. Yu, Effect of sintering conditions on particle contacts and mechanical properties of pm steels prepared from 3%Cr prealloyed powder, *Powder Metall. Prog.*, 2(2002), No. 4, p. 211.

[12] T. Marcu, A. Molinari, G. Straffelini, and S. Berg, Microstructure and tensile properties of 3%Cr–0.5%Mo high carbon PM sintered steels, *Powder Metall.*, 48(2005), No. 2, p. 139.

[13] M. Hrubovcakova, E. Dudrova, E. Hryha, M. Kabatova, and J. Harvanova, Parameters controlling the oxide reduction during sintering of chromium prealloyed steel, *Adv. Mater. Sci. Eng.*, 43(2013), p. 10413.

[14] S. Chauhan, V. Verma, U. Prakash, P.C. Tewari, and D. Khanduja, Processing of Cr–Mo alloy steel via PM route, *Mater. Today*, 3(2016), No. 9, p. 2899.

[15] P.A. Hassell and N.V. Ross, *ASM Handbook, Vol. 4C: Induction Heating and Heat Treatment*, ASM International, 1991, p. 413.

[16] K. Palaniradja, N. Alagumurthi, and V. Soundararajan, Modeling of phase transformation in induction hardening, *Open Mater. Sci. J.*, 4(2010), p. 64.

[17] A. Kusmoko, D.P. Dunne, R. Dahar, and H.J. Li, Surface treatment evaluation of induction hardened and tempered 1045 steel, *Int. J. Curr. Eng. Technol.*, 4(2014), No. 3, p. 1236.

[18] V. Rudnev, Intricacies of induction hardening powder metallurgy parts, *Heat Treat. Prog.*, Nov/Dec 2003, p. 23.

[19] H.A. Ferguson, *ASM Handbook, Vol. 4D: Heat Treating of Irons and Steels*, ASM International, 1991, p. 548.

[20] E. Hryha and L. Nyborg, Effectiveness of reducing agents during sintering of Cr-prealloyed PM steels, *Powder Metall.*, 57(2014), No. 4, p. 245.

[21] S. Chauhan, V. Verma, U. Prakash, P.C. Tewari, and D. Khanduja, Analysis of powder metallurgy process parameters for mechanical properties of sintered Fe–Cr–Mo alloy steel, *Mater. Manuf. Processeses*, 32(2017), No. 5, p. 537.

[22] M. Maalekian, *Effect of Alloying Elements in Steel (I)*, Christian Doppler Laboratory for Early Stages of Precipitation, Institute of Material Science, Welding Technology and Chipless Forming, Technical University Graz, Graz, 2007, p. 10.